GEOLOGY

Fragmentation of wall rock garnets during deep crustal earthquakes

Håkon Austrheim,[1] Kristina G. Dunkel,[1] Oliver Plümper,[2] Benoit Ildefonse,[3] Yang Liu,[2,4] Bjørn Jamtveit[1]*

Fractures and faults riddle the Earth's crust on all scales, and the deformation associated with them is presumed to have had significant effects on its petrological and structural evolution. However, despite the abundance of directly observable earthquake activity, unequivocal evidence for seismic slip rates along ancient faults is rare and usually related to frictional melting and the formation of pseudotachylites. We report novel microstructures from garnet crystals in the immediate vicinity of seismic slip planes that transected lower crustal granulites during intermediate-depth earthquakes in the Bergen Arcs area, western Norway, some 420 million years ago. Seismic loading caused massive dislocation formations and fragmentation of wall rock garnets. Microfracturing and the injection of sulfide melts occurred during an early stage of loading. Subsequent dilation caused pervasive transport of fluids into the garnets along a network of microfractures, dislocations, and subgrain and grain boundaries, leading to the growth of abundant mineral inclusions inside the fragmented garnets. Recrystallization by grain boundary migration closed most of the pores and fractures generated by the seismic event. This wall rock alteration represents the initial stages of an earthquake-triggered metamorphic transformation process that ultimately led to reworking of the lower crust on a regional scale.

INTRODUCTION

Deformation of the lithosphere by seismic slip along faults dissipates energy to the immediate surroundings as heat and elastic waves. Heat effects may occasionally cause frictional melting along the slip plane, leading to the formation of pseudotachylite, a characteristic fine-grained or glassy fault rock, interpreted as the quenched melt (*1*, *2*). Recently, it has been suggested that mechanical effects due to rapid loading, such as the formation of shiny "mirror" surfaces or pulverization of rocks without significant shear or "grinding," are diagnostic of seismic faulting (*3*, *4*). However, these features have been found only in shallow faults (*5*, *6*), and in the absence of pseudotachylites, very few criteria can be used to distinguish between unstable slip and slower creep processes along deeper faults. Here, we provide detailed descriptions of mineral microstructures formed in garnet-bearing granulites from the Bergen Arcs, western Norway, during seismic slip at deep crustal levels. Wall rock garnets reveal an intriguing coupling between crystal-plastic deformation and mass transfer during seismic slip.

The Bergen Arcs are a series of arcuate thrust sheets centered on the city of Bergen, western Norway. The investigated rocks are located in the Lindås Nappe, where anorthositic rocks are the dominant lithologies (*7*). The Lindås Nappe recrystallized to a granulite facies mineralogy characterized by plagioclase, clinopyroxene, orthopyroxene, scapolite, garnet, spinel, and minor amphibole at 930 Ma (million years ago) (*8*). During the Caledonian continent collision between Laurentia and Baltica between 420 and 440 Ma (*8*), fluid-induced eclogitization occurred in shear zones and breccias and along fractures. The estimated eclogitization conditions are ca. 650° to 700°C and 1.5 to 2.0 GPa (*9*, *10*). Pseudotachylite-filled faults with displacements of up to 0.5 m (Fig. 1A) developed in the granulites in close proximity to the eclogite facies shear zones (*11*). They may form as single veins ranging in thickness from millimeters to a few centimeters but also occur as a thin "matrix" between rotated granulite facies blocks in brecciated granulite areas that sometimes cover more than 100 m^2. The pseudotachylites often display dendritic growth of eclogite facies minerals, suggesting that faulting occurred under eclogite facies conditions. Eclogite shear zones develop from the pseudotachylites (*12*). Away from the pseudotachylite, the granulite facies garnets are chemically homogeneous and largely inclusion-free, with a restricted compositional range ($Prp_{45–56}Alm_{25–31}Grs_{16–24}$) (*13*).

RESULTS

Microstructural analysis

Microscopic observations reveal that wall rock garnets in the immediate vicinity of the pseudotachylite have a higher density of inclusions than garnets in the original granulites. We did not observe any obvious differences in the garnet microstructure on opposite sides of the fault zone. Two garnet crystals from the pseudotachylite wall rocks were selected for detailed examination by scanning electron microscopy (SEM), electron microprobe (EMP) and electron backscatter diffraction (EBSD) analysis, focused ion beam SEM (FIB-SEM), and transmission electron microscopy (TEM) (see Materials and Methods). Both garnets are ca. 1 mm in diameter and were originally part of the granulite facies anorthositic rock.

Garnet I (Fig. 1B) is in direct contact with the pseudotachylite and was cut by the fault plane so that only a "half garnet" remains as part of the wall rock. Garnet II is located about 2 mm from the pseudotachylite contact. Garnet I is transected by slightly Fe-enriched planar structures, resembling healed microfractures, some of which contain arrays of subspherical sulfide inclusions (Fig. 2, A and B) of complex chemical composition (see below). Eclogite facies mineral inclusions occur pervasively throughout the garnet domain. In contrast, Garnet II contains domains that are essentially free of mineral inclusions separated by inclusion-rich bands. The inclusion-rich parts form structures akin to a fracture network (Fig. 2C) that pervades the inclusion-free domains

[1]Physics of Geological Processes, Department of Geosciences, University of Oslo, P. O. Box 1048 Blindern, N-0316 Oslo, Norway. [2]Department of Earth Sciences, Utrecht University, Budapestlaan 4, NL-3584 CD Utrecht, Netherlands. [3]Géosciences Montpellier, UMR CNRS-UM2 5243, CC 60, Université de Montpellier, 34095 Montpellier Cedex 05, France. [4]Debye Institute for Nanomaterials Science, Utrecht University, Princetonplein 1, 3584 CC Utrecht, Netherlands.
*Corresponding author. Email: bjorn.jamtveit@geo.uio.no

(Fig. 2D). The transitions between these domains appear sharp at the resolution of the backscattered electron (BSE) images.

EBSD mapping shows that the inclusion-rich parts of the garnet invariably consist of a large number of grains (Fig. 3A), which we attribute to the fragmentation of a single crystal. In the following, we define grain boundaries as interfaces across which the garnet lattice orientations differ by >10°. Interfaces with a lattice orientation difference ≤10 degrees will be referred to as subgrain boundaries. The observed fragmentation process occurred without obvious shear deformation and associated changes of the macroscopic shape of the garnets (except for some deformation of the lower left-hand side of Garnet II; Fig. 2C). Garnet I is completely fragmented into an assembly of grains with an average diameter in the range of 6 to 9 μm. The orientations of neighboring grains are highly correlated (fig. S1), as expected during plastic deformation of the original crystal, and the corresponding pole figures (fig. S1, A and B) indicate that the grains have a strong crystallographic preferred orientation (CPO). Figure 3B further demonstrates that the smallest grains are unevenly distributed and concentrated along planar structures in Garnet I. Domains characterized by small grains are interpreted as regions subject to relatively

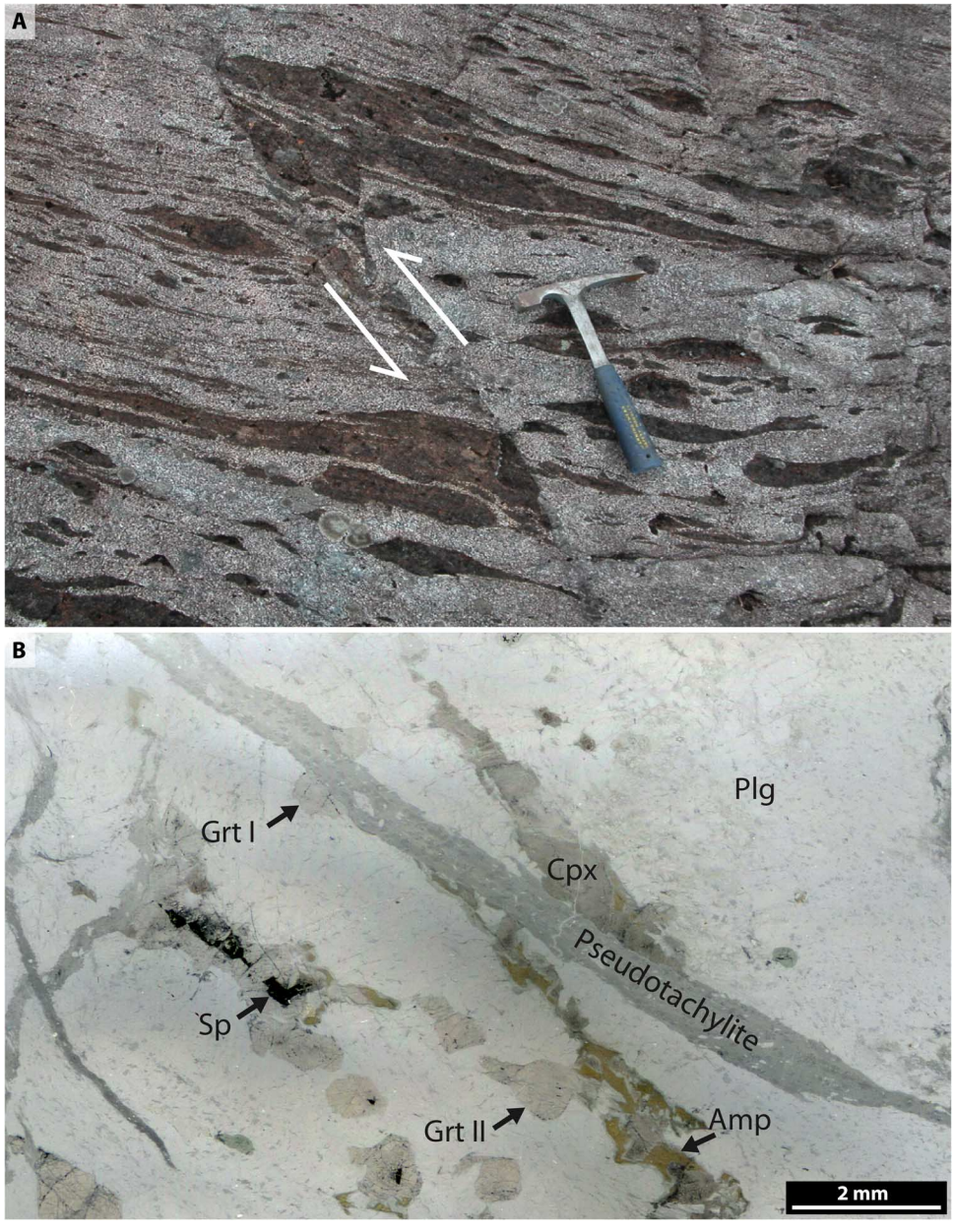

Fig. 1. Seismic faulting in the lower crust. (**A**) A fault through lower crustal granulite (arrows) produced a millimeter-thick frictional melt zone that froze to form a pseudotachylite vein with a hydrous eclogite facies mineralogy comprising dendritic garnet, kyanite, clinopyroxene (omphacite and sodic augite), and amphibole. (**B**) Photomicrograph showing the positions of the garnets studied here [Garnet I (Grt I) and II (Grt II)], with respect to a ca. 1-mm-thick pseudotachylite crosscutting the plagioclase (Plg)–rich granulite. Garnet I is part of a larger garnet that was cut off by the fault. The granulite facies assemblage also includes clinopyroxene (Cpx), amphibole (Amp), and spinel (Sp). Photo credit: Håkon Austrheim, University of Oslo.

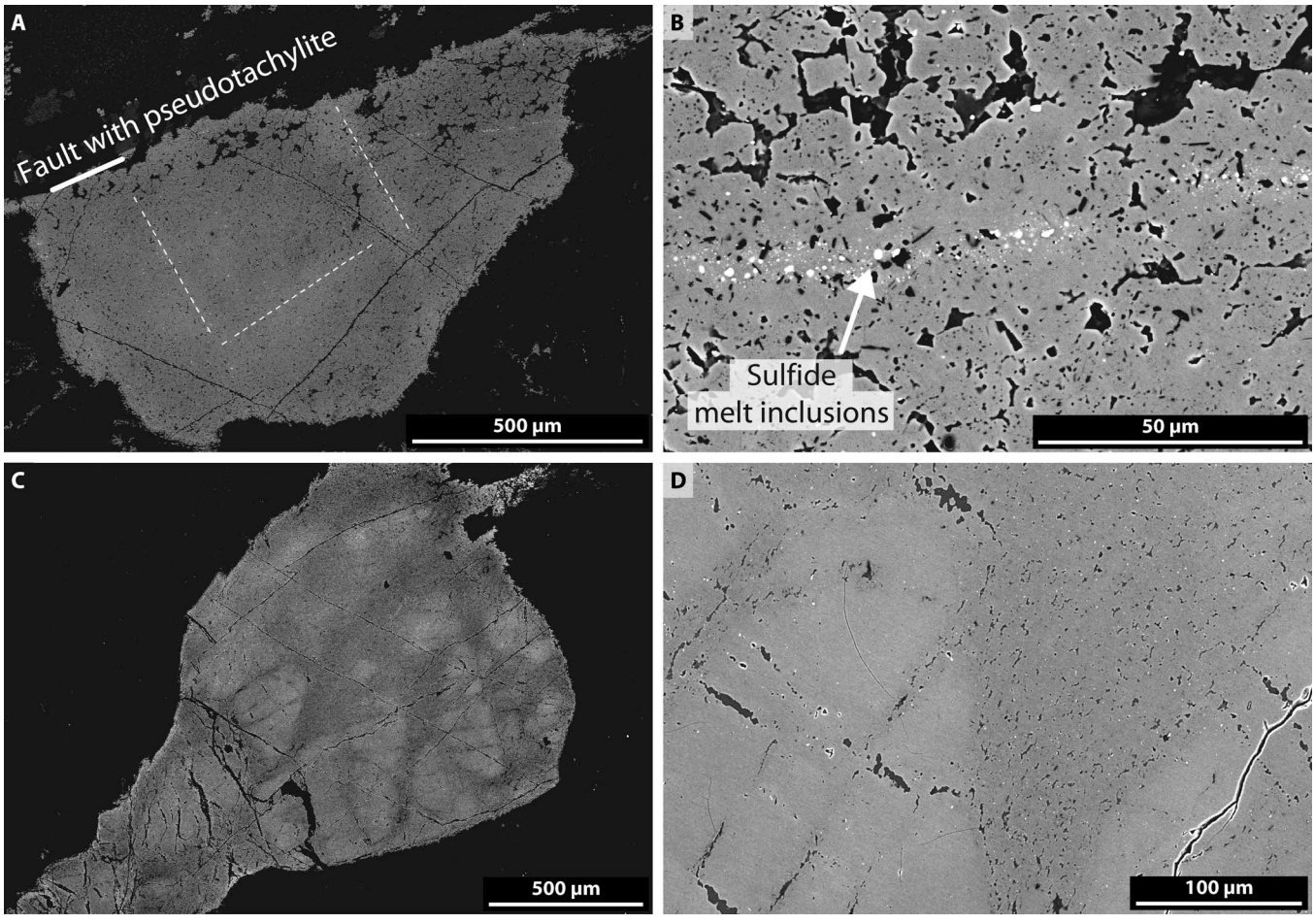

Fig. 2. BSE images of garnets. (**A**) BSE image of garnet in contact with pseudotachylite (Garnet I), revealing a high density of inclusions pervasively distributed in the garnet domain. Dashed white lines denote Fe-enriched linear sections (brighter in the BSE image). Some of these contain arrays of sulfide inclusions. (**B**) Close-up of sulfide-rich array (bright spots) through a garnet rich in inclusions of clinopyroxene, kyanite, amphibole, and dolomite (dark areas). (**C**) Garnet located ca. 2 mm from the pseudotachylite vein (Garnet II). (**D**) Close-up of the interface region separating relict (inclusion-free) garnet from the inclusion-rich domain.

high stress in systems undergoing deformation by dislocation creep (*14*). Figure 3B may thus reflect a heterogeneous stress distribution in the garnet during slip. These planar domains are often associated with arrays of sulfide-rich inclusions (Fig. 2B). However, the Ca map (Fig. 3C) illustrates that high-Ca inclusions (pyroxene and amphibole) and Ca-enriched garnet are focused outside the areas of the small grains. Garnet II contains large unfragmented domains (on the order of 100 µm in diameter) (Fig. 3D), cut by fractures rich in amphibole and clinopyroxene inclusions. However, even the unfragmented domains show internal lattice distortions and local subgrain formation focused around the inclusion-rich fractures and other, often sublinear, bands. Mineral inclusions are seen as bright areas in the Ca map (Fig. 3E) and are abundant in the inclusion-rich, fragmented domains surrounding the garnet relics. The grains and subgrains of Garnet II are, on average, somewhat smaller than those of Garnet I (2.5 to 4.0 µm in average diameter) and so are the average sizes of the mineral inclusions (see below). The strength of the CPO is similar to that in Garnet I (fig. S1, A and B).

Dislocation structures, porosity, and inclusions

FIB-SEM–assisted TEM reveals complex dislocation, (sub)grain, and inclusion/porosity substructures (see fig. S2 for the location of TEM foils excavated via FIB-SEM). Figure 4A shows part of the interface (red dashed line) between the unfragmented garnet relic and the fragmented garnet domain of Garnet II. The garnet relic contains a relatively low density of free dislocations, whereas the fragmented domain shows intense (sub)grain formation, in accordance with EBSD analysis (Fig. 3D). The intensely fragmented domain of Garnet I (Fig. 4B) exhibits grains and subgrains with internal dislocation networks encompassed by (sub)grains free of dislocations (Fig. 4, C and D). Figure 4E highlights an individual grain consisting of both an area free of dislocations and a complex dislocation network, suggesting incomplete recovery during recrystallization and annealing. Isolated submicrometer-sized pores decorate the (sub)grain boundary network in both garnets (Fig. 4F). Along with the pores, solid-phase inclusions are found (Fig. 4F and figs. S3 and S4).

Most inclusions represent the dominant eclogite facies mineralogy (clinopyroxene, clinoamphibole, kyanite, and rutile) that formed during crystallization of the frictional melt to form the pseudotachylite. However, numerous accessory minerals, such as corundum, apatite, and Fe-Ni sulfide, were also identified (Fig. 4G and fig. S5). The inclusions are too small or too intimately intergrown with other phases to enable high-quality EMP analysis. Semiquantitative analysis confirms the presence of both omphacite and sodic augite among the clinopyroxene

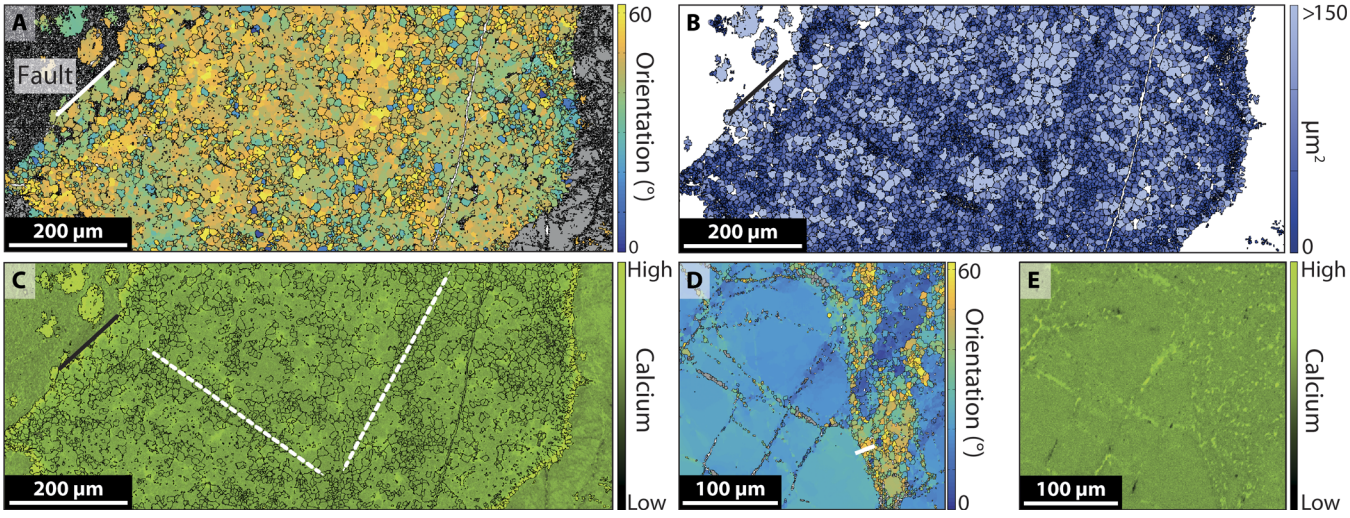

Fig. 3. EBSD images of fragmented garnet crystals. (**A**) Orientation map of garnet grains (black lines; misorientation of >10°) and subgrains within the Garnet I domain shown in Fig. 2A. Color code shows deviation from an arbitrary reference orientation. (**B**) Spatial distribution of grain sizes. Small grains (dark) are concentrated along linear features with a slight Fe enrichment [dashed lines in Fig. 2A and in (C)]. (**C**) Garnet grain boundaries superimposed on a Ca map, showing that patchy Ca enrichment is higher in areas dominated by large grains. (**D**) Orientation map for the Garnet II domain shown in Fig. 2D. The large domain (left) is a relic of the granulite facies garnets. White bar in lower right quarter denotes position of FIB cut and TEM profile shown in Fig. 4A. (**E**) Ca map of area shown in (D).

inclusions, in agreement with an observed correlation between the spatial distribution of clinopyroxene inclusions and Na (fig. S6). High-quality analyses of the eclogite facies minerals in pseudotachylites from this area have previously been reported by Austrheim and Boundy (*11*) and Aasen (*15*) and include omphacite with up to nearly 50% jadeite component.

Many inclusions are either plate-shaped and located along the (sub)grain boundaries or L-shaped and situated at grain boundary triple junctions, suggesting that the grain boundary network existed before the formation of the inclusions. In addition, chemically complex (S-, Cl-, Fe-, Na-, Si-, K-, and Zn-containing) melt inclusions frequently occur along the (sub)grain boundary network (Fig. 4G and fig. S7). A possible source of sulfur is the thermal breakdown of sulfur-rich scapolite, which locally represents as much as 5 volume % of the original granulite (*16*).

Nanotomography of inclusions

The distribution of mineral inclusions in both garnets was characterized by FIB-SEM nanotomography (see fig. S2 for nanotomography locations) (*17*). Garnet I, next to the fault, contains 7 volume % mineral inclusions (Fig. 4H), and interconnected volumes of amphibole (purple in Fig. 4H) occur along the (sub)grain boundary network. This indicates a complete wetting of the (sub)grain boundaries during fluid infiltration. In contrast, Garnet II, away from the fault, contains 2.0 to 2.5 volume % inclusions (Fig. 4I) and no identifiable interconnected areas. This indicates that infiltration of fluid and melt decreases with increasing distance from the fault. The size distribution of the inclusions has a log-normal form (fig. S8), consistent with formation via nucleation and growth (*18*).

DISCUSSION

The microstructures described above are confined to a region with a width of a few millimeters around pseudotachylite-filled fractures and arise due to seismic faulting and associated changes in the local stresses. Formation of sulfide droplets and both hydrous minerals and carbonates as inclusions in the garnets further indicates the presence of fluids and sulfide melts in these initially dry rocks during the seismic event. Preservation of original macroscopic shapes of the garnet crystals shows that the microstructures formed without substantial shear strain. In many respects, this fragmentation of garnet crystals into an assembly of smaller grains is analogous to the brittle "pulverization," which has been described in the wall rocks of shallow faults (*19*–*22*). However, the garnet pulverization observed here is associated with extensive defect generation and crystal plasticity. Fragmentation by crystal plasticity has previously been described from slip zones during rotary shear experiments in marbles (*23*) and from microshear zones in quartz in the brittle crust (*24*). A similar microstructural response to dynamic loading has been described in quartz and other minerals from impact structures (*25*–*27*) and is often referred to as "mosaicism." The mechanism behind mosaicism is still unclear, but it is often associated with planar deformation features (PDFs). PDFs have previously been described from the Bergen Arc garnets (*13*). However, the microstructures reported here do not appear to be preceded by PDFs, as described from impact-generated mosaic textures in quartz (*27*). We have chosen the term fragmentation, rather than mosaicism, to describe the origin of the structures observed here, following the terminology of Rybin *et al.* (*28*) for systems with abundant high-angle grain boundaries.

There has been extensive and pervasive mass transfer into the original garnet volumes from the main fault zone during the formation of the mineral inclusions. We believe that the Fe-enriched linear features in Garnet I, with their associated arrays of sulfide droplets and regions of small (sub)grains, have formed during an early stage. Their orientation at a high angle to the fault zone might indicate that they formed during a stage of compression normal to the fault zone. However, the eclogite facies mineral inclusions formed subsequent to the main stage of subgrain formation, and the volume occupied by these inclusions requires dilations of ca. 7.0 and 2.5% for Garnet I and Garnet II, respectively. Although these are maximum values, assuming

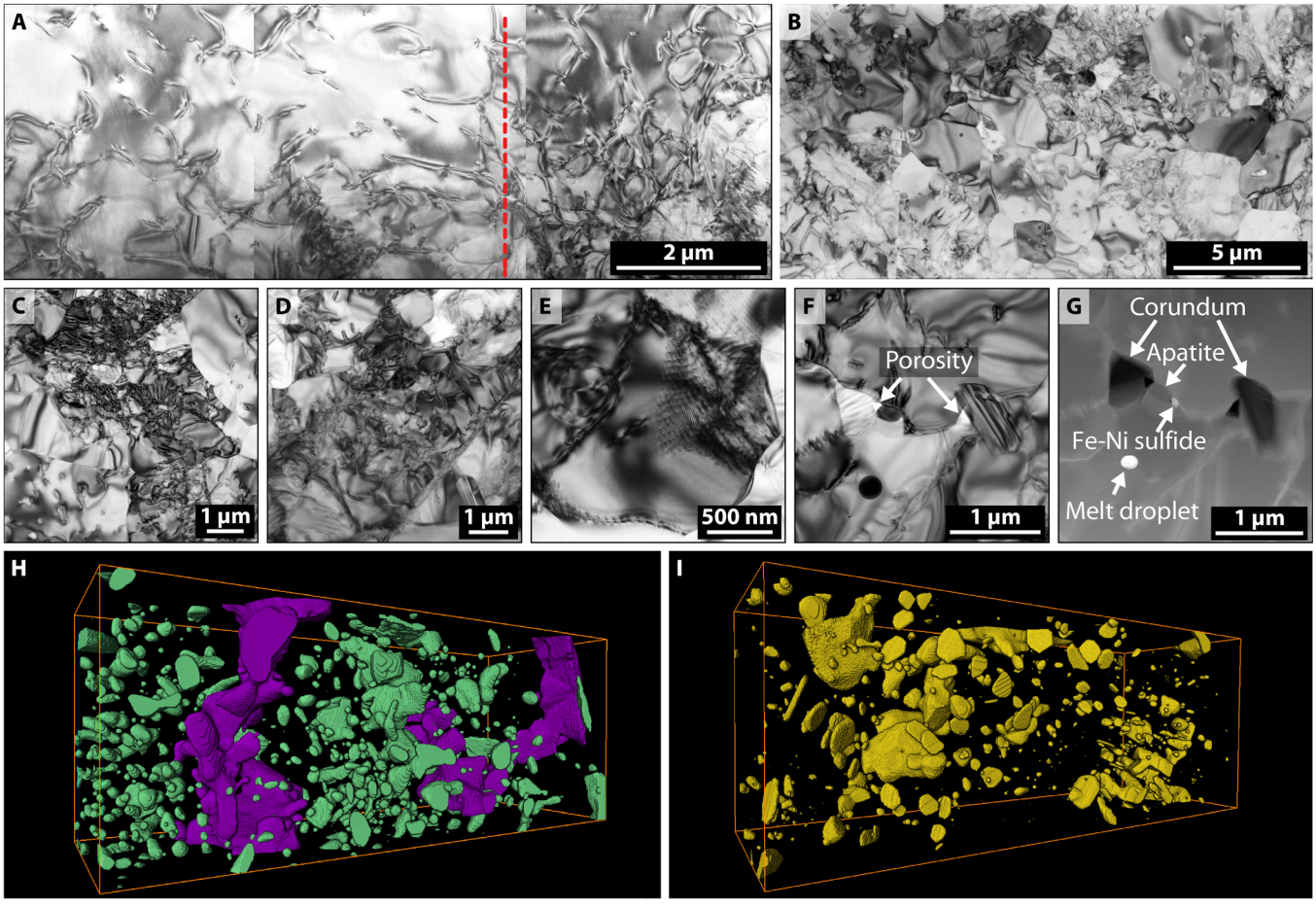

Fig. 4. Nanoscale structures of seismically fragmented garnets. (**A**) Interface (red dashed line) between relict and fragmented garnet (Garnet II). The relic shows scattered, free dislocations, whereas the fragmented domain consists of individual (sub)grains. The location of the TEM lamellae is given in Fig. 3D. (**B**) Overview of the fragmented domain in Garnet I characterized by (sub)grains with high dislocation densities and (sub)grains free of dislocations (**C** and **D**). (**E**) Garnet grain, where the lower half is dislocation-free and the upper half shows a dislocation network. (**F** and **G**) Pores and inclusions along garnet (sub)grain boundaries. (**H** and **I**) Three-dimensional (3D) visualization of inclusion network in Garnet I and Garnet II ($20 \times 20 \times 10$ μm^3). Purple area in (H) denotes interconnected amphibole along (sub)grain boundaries.

no contribution from reactions involving dissolution or chemical breakdown of the garnet itself, this amount of dilation is realistic at millimeter distances from an earthquake-related shear fracture (*29*). The temporal evolution of stress in the wall rocks during fault slip may be highly complex, depending on factors such as fault roughness, slip rate, and asymmetries of the rock properties around the fault (*21*, *29*, *30*). The microstructural observations and associated mass transport presented here may reflect that the local stresses fluctuated between compressive and dilatant during the seismic event.

Subgrain formation in natural garnets was first reported in mantle nodules by Prior *et al.* (*31*) and has since been described in high-strain zones in the Alps (*32*, *33*) and the Appalachians (*34*). In most of these cases, the garnet experienced significant shear strain, and the stress state and rate of strain are not well constrained. However, Trepmann and Stöckhert (*33*) provided strong evidence that garnets in mid-crustal mylonites from the Sesia Zone, Western Alps, had experienced "quasi-instantaneous shattering by synseismic loading" before shear deformation. To our knowledge, this study from the Bergen Arcs is the first to provide a detailed documentation of fragmentation and associated crystal plasticity in wall rock minerals without significant shear strain during an ancient earthquake in the deep crust. We propose that such microstructures may help in the identification of seismic events in ancient faults.

Although the seismicity-induced fragmentation affects only a modest volume of rock around the fault, the fluid-rock interactions taking place in the wall rocks of the slip zone in the microseconds of high and fluctuating stresses during an earthquake produce rocks of dramatically different rheological properties compared to the original rigid and strong granulites. In the Bergen Arcs area, the seismic events started a cascade of creep processes and metamorphic transformations, which eventually resulted in a massive reworking of the lower crust on regional scales during the Caledonian orogeny (*12*, *35*). The observations reported here thus represent the incipient stages of an earthquake-triggered regional metamorphism of the deep crust.

MATERIALS AND METHODS

SEM/EMP analysis

BSE images were acquired on a Hitachi SU5000 field-emission SEM, and mineral compositions were measured by wavelength-dispersive spectroscopy with a Cameca SX 100 EMP using an acceleration voltage of 15 kV and beam currents between 10 and 20 nA. Both the SEM

and EMP are located at the Department of Geosciences, University of Oslo, Norway.

Electron backscatter diffraction

Crystallographic orientations of garnet and secondary phases were determined by indexing the EBSD patterns acquired with the CamScan X500FE Crystal Probe at Géosciences Montpellier (CNRS-Université de Montpellier, France) equipped with an Oxford Nordlys EBSD detector. The Crystal Probe was used at an accelerating voltage of 15 kV and step sizes of 0.35 and 0.40 µm. EBSD patterns were indexed automatically using the AZtec software from Oxford Instruments. Qualitative energy-dispersive spectroscopy (EDS) element maps were acquired concurrently to the EBSD maps using the X-Max^N 20-mm^2 EDS detector of the Crystal Probe. Although almost all the patterns (96 and 93%) could be indexed automatically, some post-acquisition data treatment was done using the Tango software of the Channel 5 suite (HKL Technology) to remove small nonindexed areas within larger grains: Isolated pixels that are either nonindexed or indexed but surrounded by pixels assigned to a different phase were removed, and nonindexed pixels that have a minimum of six neighboring pixels with almost equal orientations were given the average of those orientations. Crystallographic orientations and grain sizes were analyzed and visualized using the MATLAB toolbox MTEX (version 4.3.1; http://mtex-toolbox.github.io) (*36*, *37*). Misorientation thresholds of 10° and 1° were used during grain and subgrain identification, respectively. Grains and subgrains smaller than 10 pixels were excluded.

Focused ion beam SEM/transmission electron microscopy

Electron-transparent thin foils were prepared for (scanning) STEM by using an FEI Helios NanoLab G3 FIB-SEM. The FIB-SEM was also used to acquire several slice-and-view series for 3D volume reconstructions. Slice imaging was carried out in BSE mode at 3 kV and 3.2 nA with a pixel size of 8 × 8 nm^2 (voxel size of 8 × 8 × 30 nm^3). All FIB-SEM nanotomography volumes were reconstructed and analyzed using FEI Avizo 9. Thin foils were investigated in an FEI Talos F200X (S)TEM equipped with four energy-dispersive x-ray spectroscopy detectors (Super-EDX). All FIB-SEM and TEM analyses were carried out at the Electron Microscopy Square, Utrecht University.

SUPPLEMENTARY MATERIALS

Supplementary material for this article is available at http://advances.sciencemag.org/cgi/content/full/3/2/e1602067/DC1

fig. S1. Strong CPOs of fragmented garnet.
fig. S2. Position of nanotomography volumes and TEM lamellae.
fig. S3. TEM images of pores and inclusions.
fig. S4. Inclusion phases in fragmented garnet.
fig. S5. Sulfide inclusion in garnet.
fig. S6. Clinopyroxene inclusion distribution and composition.
fig. S7. Melt inclusion along the (sub)grain boundary in fragmented garnet.
fig. S8. Size distribution of inclusions.

REFERENCES AND NOTES

1. R. H. Sibson, Generation of pseudotachylyte by ancient seismic faulting. *Geophys. J. Int.* **43**, 775–794 (1975).
2. J. D. Kirkpatrick, C. D. Rowe, Disappearing ink: How pseudotachylytes are lost from the rock record. *J. Struct. Geol.* **52**, 183–198 (2013).
3. M. Fondriest, S. A. F. Smith, T. Candela, S. B. Nielsen, K. Mair, G. Di Toro, Mirror-like faults and power dissipation during earthquakes. *Geology* **41**, 1175–1178 (2013).
4. B. A. Verberne, O. Plümper, D. A. M. de Winter, C. J. Spiers, Superplastic nanofibrous slip zones control seismogenic fault friction. *Science* **346**, 1342–1344 (2014).
5. N. Wechsler, E. E. Allen, T. K. Rockwell, G. Girty, J. S. Chester, Y. Ben-Zion, Characterization of pulverized granitoids in a shallow core along the San Andreas Fault, Littlerock, CA. *Geophys. J. Int.* **186**, 401–417 (2011).
6. S. Siman-Tov, E. Aharonov, A. Sagy, S. Emmanuel, Nanograins form carbonate fault mirrors. *Geology* **41**, 703–706 (2013).
7. C. Kolderup, N. Kolderup, Geology of the Bergen Arc system. *Bergens Mus. Skr.* **20**, 137 (1940).
8. B. Bingen, W. J. Davis, H. Austrheim, Zircon U-Pb geochronology in the Bergen arc eclogites and their Proterozoic protoliths, and implications for the pre-Scandian evolution of the Caledonides in western Norway. *Geol. Soc. Am. Bull.* **113**, 640–649 (2001).
9. B. Jamtveit, K. Bucher-Nurminen, H. Austrheim, Fluid controlled eclogitization of granulites in deep crustal shear zones, Bergen arcs, Western Norway. *Contrib. Mineral. Petrol.* **104**, 184–193 (1990).
10. T. M. Boundy, D. M. Fountain, H. Austrheim, Structural development and petrofabrics of eclogite facies shear zones, Bergen Arcs, western Norway: Implications for deep crustal deformational processes. *J. Metam. Geol.* **10**, 127–146 (1992).
11. H. Austrheim, T. M. Boundy, Pseudotachylytes generated during seismic faulting and eclogitization of the deep crust. *Science* **265**, 82–83 (1994).
12. H. Austrheim, Fluid and deformation induced metamorphic processes around Moho beneath continent collision zones: Examples from the exposed root zone of the Caledonian mountain belt, W-Norway. *Tectonophysics* **609**, 620–635 (2013).
13. H. Austrheim, M. Erambert, T. M. Boundy, Garnets recording deep crustal earthquakes. *Earth Planet. Sci. Lett.* **139**, 223–238 (1996).
14. J.-P. Poirier, *Creep of Crystals: High-Temperature Deformation Processes in Metals, Ceramics and Minerals* (Cambridge Univ. Press, 1985).
15. H. S. Aasen, thesis, University of Oslo (2013).
16. J. K. Porter, H. Austrheim, Sulphide formation from granulite-facies S-rich scapolite breakdown. *Terra Nova* **29**, 29–35 (2017).
17. Y. Liu, H. E. King, M. A. van Huis, M. R. Drury, O. Plümper, Nano-tomography of porous geological materials using focused ion beam-scanning electron microscopy. *Minerals* **6**, 104 (2016).
18. D. E. Kile, D. D. Eberl, A. R. Hoch, M. M. Reddy, An assessment of calcite crystal growth mechanisms based on crystal size distributions. *Geochim. Cosmochim. Acta* **64**, 2937–2950 (2000).
19. B. Wilson, T. Dewers, Z. Reches, J. Brune, Particle size and energetics of gouge from earthquake rupture zones. *Nature* **434**, 749–752 (2005).
20. O. Dor, Y. Ben-Zion, T. K. Rockwell, J. Brune, Pulverized rocks in the Mojave section of the San Andreas Fault Zone. *Earth Planet. Sci. Lett.* **245**, 642–654 (2006).
21. M.-L. Doan, G. Gary, Rock pulverization at high strain rate near the San Andreas fault. *Nat. Geosci.* **2**, 709–712 (2009).
22. T. M. Mitchell, Y. Ben-Zion, T. Shimamoto, Pulverized fault rocks and damage asymmetry along the Arima-Takatsuki Tectonic Line, Japan. *Earth Planet. Sci. Lett.* **308**, 284–297 (2011).
23. E. Spagnuolo, O. Plümper, M. Violay, A. Cavallo, G. Di Toro, Fast-moving dislocations trigger flash weakening in carbonate-bearing faults during earthquakes. *Sci. Rep.* **5**, 16112 (2015).
24. M. Bestmann, G. Pennacchioni, S. Nielsen, M. Göken, H. de Wall, Deformation and ultrafine dynamic recrystallization of quartz in pseudotachylyte-bearing brittle faults: A matter of a few seconds. *J. Struct. Geol.* **38**, 21–38 (2012).
25. F. Dachille, P. Gigl, P. Simons, Experimental and analytical studies of crystalline damage useful for the recognition of impact structures, in *Shock Metamorphism of Natural Materials*, B. French, N. Short, Eds. (Mono Book Corp., 1968), pp. 555–569.
26. D. Stöffler, F. Langenhorst, Shock metamorphism of quartz in nature and experiment: I. Basic observation and theory. *Meteoritics* **29**, 155–181 (1994).
27. C. A. Trepmann, Shock effects in quartz: Compression versus shear deformation—An example from the Rochechouart impact structure, France. *Earth Planet. Sci. Lett.* **267**, 322–332 (2008).
28. V. V. Rybin, N. Y. Zolotorevskii, E. Ushanova, Fragmentation of crystals upon deformation twinning and dynamic recrystallization. *Phys. Met. Metallogr.* **116**, 730–744 (2015).
29. Z. Reches, T. A. Dewers, Gouge formation by dynamic pulverization during earthquake rupture. *Earth Planet. Sci. Lett.* **235**, 361–374 (2005).
30. J. N. Brune, S. Brown, P. A. Johnson, Rupture mechanism and interface separation in foam rubber models of earthquakes: A possible solution to the heat flow paradox and the paradox of large overthrusts. *Tectonophysics* **218**, 59–67 (1993).
31. D. J. Prior, J. Wheeler, F. E. Brenker, B. Harte, M. Matthews, Crystal plasticity of natural garnet: New microstructural evidence. *Geology* **28**, 1003–1006 (2000).
32. M. Bestmann, G. Habler, F. Heidelbach, M. Thöni, Dynamic recrystallization of garnet and related diffusion processes. *J. Struct. Geol.* **30**, 777–790 (2008).
33. C. A. Trepmann, B. Stöckhert, Cataclastic deformation of garnet: A record of synseismic loading and postseismic creep. *J. Struct. Geol.* **24**, 1845–1856 (2002).

34. M. A. Massey, D. J. Prior, D. P. Moecher, Microstructure and crystallographic preferred orientation of polycrystalline microgarnet aggregates developed during progressive creep, recovery, and grain boundary sliding. *J. Struct. Geol.* **33**, 713–730 (2011).
35. H. Austrheim, Eclogitization of lower crustal granulites by fluid migration through shear zones. *Earth Planet. Sci. Lett.* **81**, 221–232 (1987).
36. F. Bachmann, R. Hielscher, H. Schaeben, Grain detection from 2d and 3d EBSD data—Specification of the MTEX algorithm. *Ultramicroscopy* **111**, 1720–1733 (2011).
37. R. Hielscher, H. Schaeben, A novel pole figure inversion method: Specification of the MTEX algorithm. *J. Appl. Cryst.* **41**, 1024–1037 (2008).

Acknowledgments: We thank L. Angheluta, A. Malthe-Sørenssen, P. Meakin, and A. Putnis for discussions and comments on the paper. M. Erambert and B. Løken Berg assisted during EMP and SEM work, C. Nevado and D. Delmas provided high-quality thin-section polishing, and F. Barou assisted with EBSD measurements. Insightful reviews by two anonymous reviewers significantly improved the paper. **Funding:** This project was supported by the European Union's Horizon 2020 Research and Innovation Programme under the European Research Council advanced grant agreement no. 669972 "Disequilibrium Metamorphism (DIME)" to B.J. and the People Programme (Marie Curie Actions) of the European Union's Seventh Framework Programme FP7/2007-2013 under the Research Executive Agency grant agreement no. 608001 "ABYSS." O.P. was supported through a Veni grant (863.13.006) awarded by the Netherlands Organisation for Scientific Research. Y.L. was supported by the Utrecht University "Sustainability" strategic scheme funding. **Author contributions:** B.J. and H.A. developed the conceptual idea for the study. H.A. did the fieldwork and sampling. H.A., B.J., and K.G.D. did the petrographic analysis and electron microscopy. K.G.D. and B.I. did the EBSD work. O.P., Y.L., and K.G.D. did the FIB and TEM studies. B.J. wrote the paper, with contributions from H.A., K.G.D., and O.P. **Competing interests:** The authors declare that they have no competing interests. **Data and materials availability:** All data needed to evaluate the conclusions in the paper are present in the paper and/or the Supplementary Materials. Additional data related to this paper may be requested from the authors.

Submitted 30 August 2016
Accepted 25 January 2017
Published 22 February 2017
10.1126/sciadv.1602067

Citation: H. Austrheim, K. G. Dunkel, O. Plümper, B. Ildefonse, Y. Liu, B. Jamtveit, Fragmentation of wall rock garnets during deep crustal earthquakes. *Sci. Adv.* **3**, e1602067 (2017).

ScienceAdvances
AAAS

Fragmentation of wall rock garnets during deep crustal earthquakes

Håkon Austrheim, Kristina G. Dunkel, Oliver Plümper, Benoit Ildefonse, Yang Liu and Bjørn Jamtveit (February 22, 2017)

Sci Adv 2017, 3:.
doi: 10.1126/sciadv.1602067